Estimating the Groundwater Storage from the Electrical Resistivity Measurements in Wadi El-Natrun Area, Western Desert, Egypt

Abdallah Ibrahim Ammar

Research Institute for Groundwater, National Water Research Center, El-Kanater El-Khairiya, Cairo, Egypt.
Abdallah_ammar_708@hotmail.com

Abstract: Forty-three vertical electrical sounding stations (VESes) were measured in Wadi El-Natrun area, northern western desert. The analysis of the given well log data was used to estimate the groundwater storage. These VESes were interpreted to determine the subsurface layers and the true resistivities, lithologies and thicknesses variations of such layers. The result of this geoelectrical analysis is the subdivision of the shallow section into five geoelectric layers throughout the study area, except in some parts, where the surface layer disappeared; and the fifth layer is not reached. These layers varied in their resistivities from very low to high values. However, the groundwater is generally contained in the second layer of the unconfined Nile Delta aquifer (Quaternary period), in the third and fourth layers of the confined and semi-confined Wadi El-Natrun aquifer (Pliocene period), then in the fifth layer of the Moghra aquifer (Lower Miocene period). Also, the effective zones of the second, third and fourth layers were separated from the electrical interpretations. However, the variation in the net and effective thickness of each layer was calculated and represented in maps. The well log data of the resistivity, SP and gamma-ray logs were used for evaluating the rock units encountered in fifteen wells. The results of these data arrive at determining the shale and non-shale contents, water saturation and the effective zones as petrophysical parameters to the second, third and fourth layers. However, the variation in the water saturation percentages, net thickness and effective thickness was represented in maps. Then, the statistical analysis from the true resistivity that derived from the geoelectric analysis, and water saturation that deduced from the well log analysis, was carried out, only to the third layer. At the end, a comparison between the net and effective thickness values from the electric and well log interpretations was made, and then by applying the resulted mathematical equations, the groundwater amounts were calculated to the three layers. The results of these calculations showed that, the third layer as high groundwater content, then the fourth layer, but the second layer contains the least amounts. Therefore, the electrical resistivity measurements can be used for estimating the groundwater amounts in case of availability the geological information and the well log data are not available. [Journal of American Science 2010;6(10):492-502]. (ISSN: 1545-1003).

Keywords: Vertical Electrical Sounding Stations (VESes); Geoelectrical; Groundwater Storage; Western Desert

1. Introduction

The study area lies in the northeastern corner of the Western Desert, to the west of the Nile Delta. It is bounded by longitudes 30° 03` 19`` and 30° 37` 6.3`` E and latitudes 30° 13` 51`` and 30° 36` 13`` N, or stretched between kilometer 78 to kilometer 136 at the Cairo-Alexandria Desert Road from Cairo city toward the northwestern direction. Wadi El-Natrun depression extends parallel to Cairo-Alexandria Desert Road and it is located about 86km North West of Cairo city (Fig.1). The surface and subsurface geologic information of the study area are available and contained in the works of Said (1962), Shata et al. (1962), El-Fayoumy (1964), El-Shazly et al. (1975 and 1978) and others.

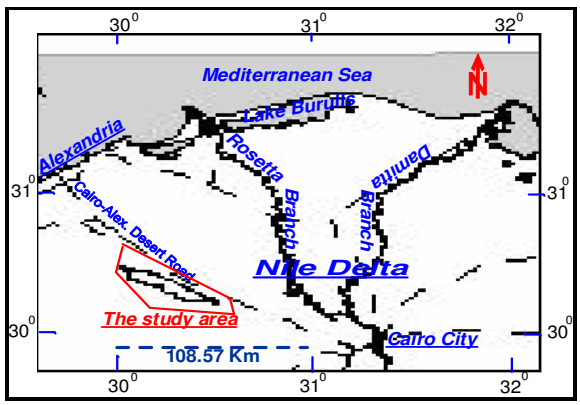

Figure (1) Location map of the study area.

I) Geomorphology

The study area, having low relief, occupies a portion of the initial Nile Delta basin and it is western fringes. In this area, there are several geomorphic units. These units are the young alluvial plain occupies much of the present flood plain of the Nile Delta and it is underlain by a silty clay layer. Its elevation varies from 12m to 14m (+MSL). The old alluvial plain occupies the area stretched between Wadi El-Natrun depression on the western side and Rosetta branch on the eastern side, and it underlain by dark brown gravel and coarse sand. Its elevation ranges between 50m and

20m (+MSL). The structural plain occupies the area to the south and southeast of Wadi El-Natrun, where the surface of this plain is underlain by sandstone beds. Its elevation varies from about 200m to 100m (+MSL). Wadi El-Natrun depression result from morpho-tectonic activities and its elevation is close to sea level.

II) Regional geology

Most of the area is occupied by Late Cenozoic rocks; where the Cenozoic Era is classified into two periods, the Quaternary period and the Tertiary period. The Tertiary period includes the Pliocene, lower Miocene and Oligocene series. The Cenozoic section is dominated by clastic sediments and it is rather thin and hardly exceeds 200m.

(i) Quaternary period

The Quaternary period includes the Holocene age and the Pleistocene age. The Holocene age is characterized by four rock units:- *The first rock unit* is the sand dunes and surficial deposits and its thickness is ranged between 10m and 30m. *The second rock unit* is the sabkha deposits and its thickness is less than 10m. *The third rock unit* is the silty and sandy clay, with a thickness of +30m. Finally, *the fourth rock unit* is the undifferentiated Quaternary, where the thickness is +20m. The Pleistocene is characterized graded sand and gravel, that intercalated by clay lenses. The thickness is ranged between 100m and 250m or even 300m.

(ii) Tertiary period

The Tertiary period is characterized by four rock units, as the alternating sandstone and clay with limestone at the top of Hagif and Hanzi Formations of *the first rock unit* during the Pliocene age. Its thickness is +130m and composed of clay in the surface determining the base of the Nile Delta. *The second rock unit* is the coarse sandstone and gravel with clay intercalations of the Lower Miocene age "Moghra Formation" and its thickness is +600m and increases to be 900m to the northwest". *The third rock unit* is the sand and gravel layers (Oligocene age), where the thickness is 100m. *The fourth rock unit* is mainly in the subsurface; its thickness is varied from 100m to 400m and is formed from a sequence of shale (Oligocene age).

III) Hydrogeology

From the previous hydrogeological studies, the West Delta area is characterized by three aquifer systems. These aquifers are:-

(i) Quaternary alluvial aquifer system (Nile Delta aquifer).
(ii) Pliocene fluvio-marine aquifer system (Wadi El-Natrun aquifer).
(iii) Lower Miocene fluvio-marine aquifer system (Moghra aquifer).

The first and second aquifers will be discussed because they are the two main aquifers under study as follow:-

(i) The Nile Delta aquifer system: It covers the greater portion of the area to the north and northeast sides. This aquifer is considered the main aquifer, not only at this area, but almost allover the delta region. However, there is more than one hydrogeological unit share together in the formation of this aquifer. It is overlain by silty clay layer "Semi-confined layer" in the Nile Delta area, but this layer is appears in the desert areas to the west, where the aquifer is unconfined. The base of this aquifer consists of a clay layer (Pliocene) having a thickness exceeds 100m and it acts as an aquiclude (it will be discussed on Figure 3).

This aquifer is recharged continuously from the Nile itself, from the canals and through the infiltration of excess irrigation water. But, the discharge take place through a part of the Rosetta branch, through the main canals and through the extraction from the drilled wells, and this aquifer is characterized by low salinity fresh water, which is generally less than 1000ppm.

(ii) The Wadi El-Natrun aquifer system: It occupies the northwestern part of the area, where the depth increases from W to E and from S to N "from Wadi El-Natrun to the Nile Delta". The groundwater of this aquifer exists under both the confined and semi-confined conditions. This aquifer is underlain by either a thick clay beds "Pliocene aquiclude" or by the Lower Miocene sands "Moghra Formation" (it will be discussed on Figure 3).

This aquifer is recharged from the Nile Delta aquifer from the excess irrigation water and some authors believed that, this aquifer is recharged from the Moghra aquifer "underlying it" and from local rain storms. But, the discharging may result from a lateral flow towards Wadi El-Natrun depression, which acts as a natural discharging area of the Nile Delta aquifer or take place through the natural springs, open galleries, drilled wells, seepage zones, evaporation and evapotranspiration. The salinity of this aquifer is ranged between 800ppm and 5000ppm.

2. Electrical Analysis:

By the Schlumberger array, a forty-three vertical electrical soundings (VESes) [with AB/2 ranged between 400m and 1000m] were carried out in the area of study by using JESSE electric instrument

through Wadi El-Natrun project by RIGW staff at locations permitting the construction of seventeen geoelectric cross sections. Each cross section passes through a number of VESes, added to the available water wells (Fig. 2).

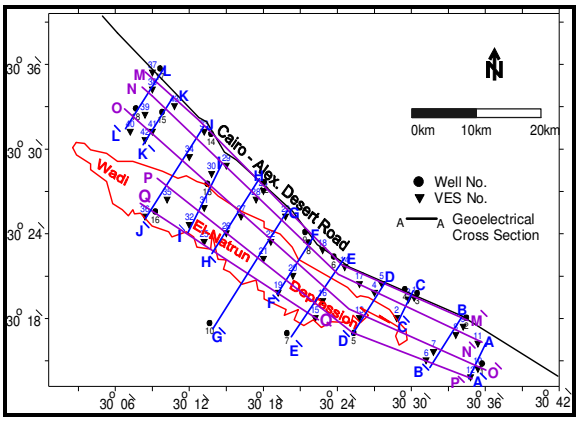

Figure (2) Wells, vertical electrical soundings (VESes) and geoelectrical cross sections distribution map of the study area.

I) Quantitative interpretation of the field data

The quantitative interpretation of the geoelectrical data obtained for the present study includes the following:

(1) Interpretation of the vertical electrical sounding curves (VESes) using ZOHDY'S technique (1989) and RINVERT'S Software program (1999).

(2) Construction and analysis of the geoelectrical cross sections.

(3) Construction of the net and effective thickness maps of the recorded geoelectric layers.

i) Results of the interpretation

The results of quantitative interpretation of the vertical electrical sounding curves reveal the number of layers in Wadi El-Natrun area varies from three to five layers. Generally, the true resistivity values of these layers are ranged between very low (2Ω.m) and high values (982.5Ω.m), and the thicknesses are varied from (0.9m) to (197.3m). The reported lithologies of the five layers are as follow; *the first layer* consists of sands, gravels and rock fragments and missed in some parts as surface layer; *the second layer* is formed from marly and shaly sand, and in some parts include lenses of shale (Nile Delta aquifer); *the third layer* is made up of clayey and sandy gravels (Wadi El-Natrun aquifer) and changed to clays (Pliocene clay) at the middle part of the study area; *the fourth layer* is composed of clayey sands and gravels (Wadi El-Natrun aquifer) and *the fifth layer* is constituted from sandstones (Moghra aquifer). All the previous layers were recorded and discussed on the profile (I-I`), which considered as a traverse cross section (Fig. 3).

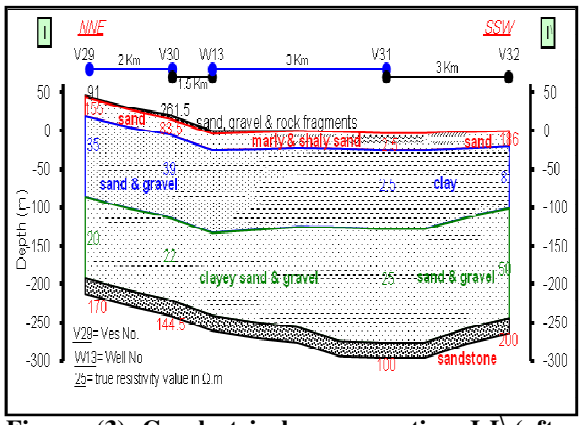

Figure (3) Geoelectrical cross section I-I` (after Ammar, 2002).

ii) Estimating the net and effective thicknesses from the geoelectric analysis.

Generally, the construction of the net and effective thickness maps from the geoelectric data of the detected layers depends upon their rock and water contents. For these reasons, if the resistivity values of the layer under investigations had reflected the occurrence of low water content in the pores of this layer or this layer was dry or has high content of shales, it will be excluded and do not take into account. Then, the net thickness maps will be constructed to estimate the net thickness variation of the saturated layers. But, the effective thickness maps will be constructed to determine the effective variation of the saturated clastic zones.

a) Net and effective thickness maps of the second geoelectric layer

These maps (Figs. 4&5) are constructed from the geoelectric data to delineate the thicknesses of the effective zones of this layers that by isolating the high true resistivity values, which reflected the dryness of the formation. Also, the very low or low true resistivity values, which referred to the occurrence of high shale content, were separated. Generally on this map (Fig. 5), the thicknesses of the effective zones increase toward the northern and northeastern directions, as located in the B and E sites, where the recharging by the surface water increases and decreases toward the southern, southwestern and northwestern directions, as located in the A, C and D sites of the study area. The previous increase and decrease were reflected by the medium and high resistivity values of this layer, respectively.

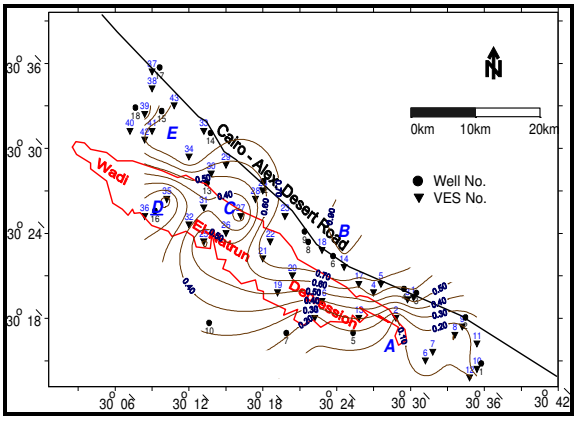

Figure (4) Net thickness map of the second geoelectric layer from the geoelectric analysis.

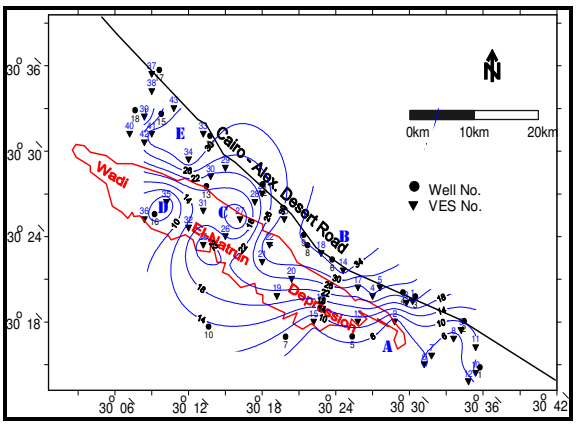

Figure (5) Effective thickness map of the second geoelectric layer from the geoelectric analysis.

b) Net and effective thickness maps of the third geoelectric layer

These maps (Figs. 6&7) are constructed from the geoelectric data by the same mentioned way. The thicknesses of the effective zones (Fig. 7) increase toward the northeastern directions, where the thickness of the Quaternary aquifer increases and decreases toward the southwestern and northwestern directions and to the southern and southeastern directions of the study area. The previous increase of this thickness appears in site B, but the decrease clears in sites A, D and C.

c) Net and Effective thickness maps of the fourth geoelectric layer

On these maps (Figs. 8&9), the sites A, C and D reflect the decrease of the effective zones. This decrease is toward the northeastern and northwestern directions. But the site B, which occurred in the southwestern part, reflects the increase of the effective zones.

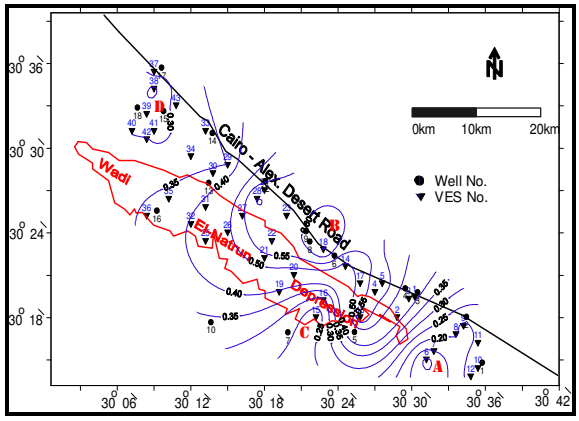

Figure (6) Net thickness map of the third geoelectric layer from the geoelectric analysis.

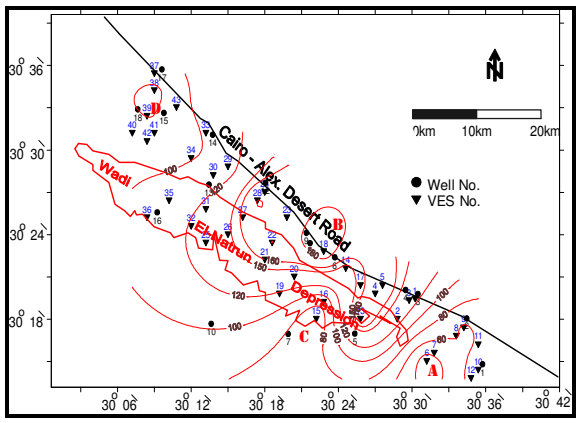

Figure (7) Effective thickness map of the third geoelectric layer from the geoelectric analysis.

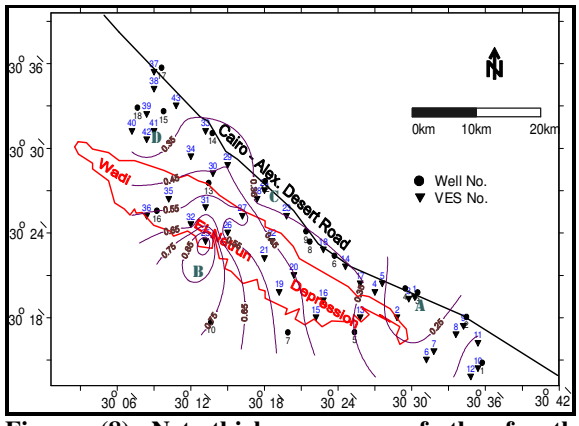

Figure (8) Net thickness map of the fourth geoelectric layer from the geoelectric analysis.

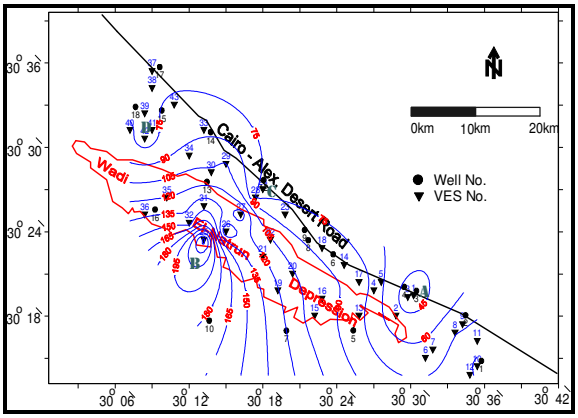

Figure (9) Effective thickness map of the fourth geoelectric layer from the geoelectric analysis.

3. Well Logging Interpretation

I) Well logging data

The present study used the available well logs (SP, Normal Resistivity and Gamma-ray) of fifteen water wells scattered in the study area (Fig. 2). Fifteen composite logs are prepared and zonation of these logs on the basis of varying deflections of the different records is done. The depth and thickness of each zone are calculated. Also, the different records of the Spontaneous Potential (mv), Short Normal (16") and Long Normal (64") resistivities (Ω.m), and Gamma-ray (G.P.S) are calculated for each zone**.**

i) Output Data

a) Shale volume (V_{sh}%): In the present study, the volume of shale (V_{sh}%) is calculated for each zone of the different composite logs, utilizing the gamma-ray logs, by using the following equation:

$$V_{sh} = \frac{GR_{log} - GR_{min}}{GR_{max} - GR_{min}} \quad \ldots\ldots\ldots\ldots\ldots\ldots\ldots\ldots (1)$$

where: V_{sh} is the volume of shale.

GR_{log} is the one measured gamma-ray value.

GR_{max} is the maximum gamma-ray value (shale zone).

GR_{min} is the minimum gamma-ray value (clean zone).

On the basis of the volume of shale percentage of each zone, the rock zones can be divided into three categories, as follows:-

- Clean rock: where $V_{sh} < 10\%$;
- Shaly rock: where $10\% < V_{sh} < 33\%$;
- Shale rock: where $V_{sh} > 33\%$.

From these, the clean zones and the shaly zones are considered the interesting zones, which reveal the effective zones in the present study. For each effective zone, the saturation of water is calculated as follows:

b) Water saturation (S_w%): The water saturation of the principal effective zones in each layer is calculated graphically using the maximum separation between the short-normal (16") and the long-normal (64") resistivity deflections opposite to the effective zones, where these zones are fully saturated with water (100% saturated with water).

From that, the water saturation (S_w%) for each effective zone in each layer will be ranged between 0% and 100% ($0\% < S_w < 100\%$). Also, the water saturation (S_w%) of the fluid in any zone of the layer will be considered the ratio of the volume occupied by the fluid (V_w) at that zone to the total pore volume (V_p), as expressed by the maximum separation of the resistivity logs, where $S_w\% = \frac{V_w}{Vp}$, i.e it is the fraction of porosity, that occupied by the particular fluid. Thus, the following ratio will be used:

$$0\% < S_w < 100\%: \; S_w\% = 100\,\frac{Vw}{Vp} \quad \ldots\ldots\ldots\ldots\ldots\ldots (2)$$

All these parameters (depth, thickness, Vsh and S_w) are used at this study to evaluate the vertical distribution of groundwater saturation in each effective zone and in each layer of the studied wells. The weighted net thicknesses (H_{net}) and the weighted water saturations (S_w) of the evaluated layers in the studied wells of the investigated area are calculated as follows:

$$\text{Net thickness } (H_{net}) = \frac{h_1 + h_2 + h_3 + \ldots + h_n}{H} \quad \ldots\ldots (3)$$

where: h_1, h_2, h_3, ...,h_n are the calculated thicknesses of the different effective zones of the studied layers.

H is the calculated total thickness of the studied layers.

$$\text{And} \quad S_w = \frac{S_{w1}h_1 + S_{w2}h_2 + S_{w3}h_3 + \ldots + S_{wn}h_n}{H} \quad \ldots\ldots (4)$$

where: S_{w1}, S_{w2}, S_{w3}, ...,S_{wn} are the calculated water saturations for the different zones of the studied layers.

$S_{w1}h_1$, $S_{w2}h_2$, $S_{w3}h_3$.....,$S_{wn}h_n$ are the water saturations of the effective zones thicknesses of the studied layers.

Finally; the present study used these calculated parameters (h_{ef}, H_{net} and S_w) of each layer for preparing nine maps to evaluate the lateral variations of these parameters throughout the study area.

II) Iso-parametric maps

i) Water saturation maps

Three maps are constructed, by using the calculated percentages of water saturation (S_w%) of the effective zones, for the second, third and fourth

layers of the studied section. These maps are very useful to give a clear picture about the lateral variation of the water occurrences in the water-bearing layers of the succession and help to indicate the most promising sites of high water saturation throughout the study area.

a) Water saturation map of the second geoelectric layer

This map (Fig. 10) reveals the presence of three anomalous sites (A, B and C). Two of them (A and C sites), that occupy the extreme parts of the area, reflect the presence of low percentage of water saturation, while the third one (B), that locates the central part, reveals the presence of high percentage of water saturation (considerable water accumulation).

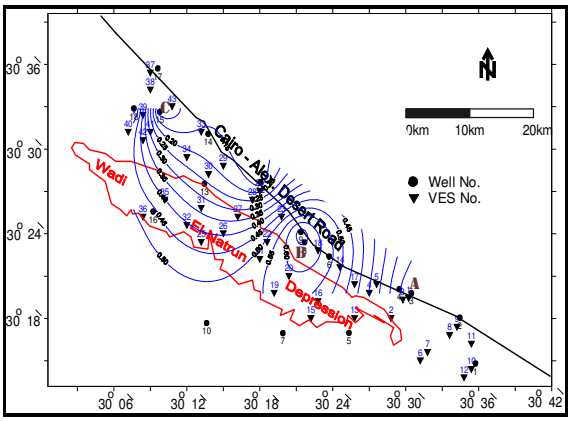

Figure (10) Water saturation map of the second geoelectric layer (after Ammar, 2002).

b) Water saturation map of the third geoelectric layer

This map (Fig. 11) shows four sites of high percentages of water saturation (A, B, C, and D). But, the other sites (E, F, and G) are of low percentages of water saturation. From these, the western, southern and northern parts of the study area are considered the best sites to water accumulations at this layer.

c) Water saturation map of the fourth geoelectric layer

This map (Fig. 12) exhibits some sort of analogy for the water saturation sites with those of the second geoelectric layer (Fig. 10), in which among three sites reported in this layer (A, B and C), (A) is the maximum, while the other two (B and C) are the minimum.

However, similarity in the distribution of the high and low water saturation anomalies between the second and fourth layers, with the dissimilarity of these in the third layer, introduces another evidence for separating the third and fourth layers from being indivisible bigger one.

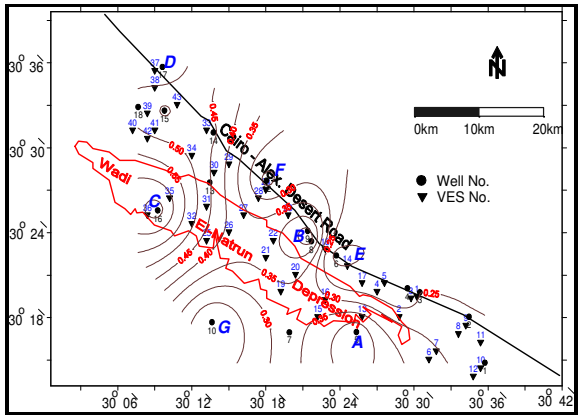

Figure (11) Water saturation map of the third geoelectric layer (after Ammar, 2002).

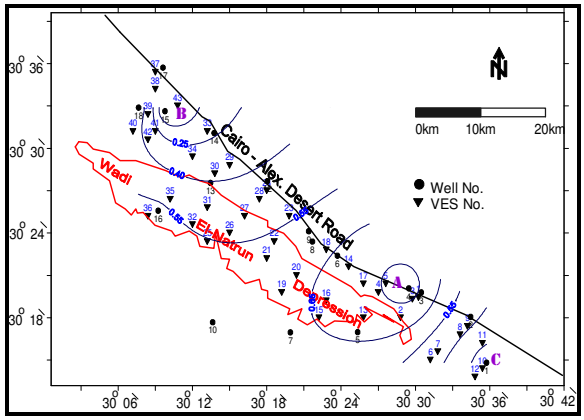

Figure (12) Water saturation map of the fourth geoelectric layer (after Ammar, 2002).

ii) Net and effective thicknesses maps

The net and effective thicknesses maps are constructed to show the lateral variations of the net and effective zones thicknesses throughout the study area of the evaluated layers at the sites of drilling wells. These maps are drawn for the second, third and fourth layers to reflect their thickenings and thinnings across the study area.

a) Net and effective thicknesses maps of the second geoelectric layer

These maps (Figs. 13 & 14) are constructed to show the lateral variations of the net and effective zones thicknesses of the second layer. There are three thickening sites (A, B and C) at the southeastern and northwestern parts of the area of study. Also, there are two thinning sites (D and E) occupying the central and southeastern parts of the concerned area. However, the northwestward increase of the total net thickness of this layer is observed, reflecting a comparable subsidence of the basin of deposition at this direction,

consequently increasing the probability of producing groundwater from the wells drilled in that direction.

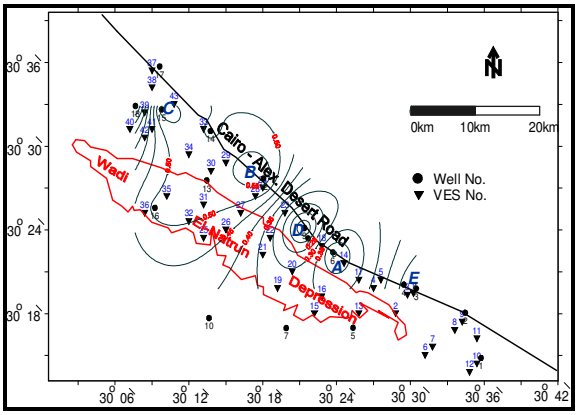

Figure (13) Net thickness map of the second geoelectric layer from the well logging analysis (after Ammar, 2002).

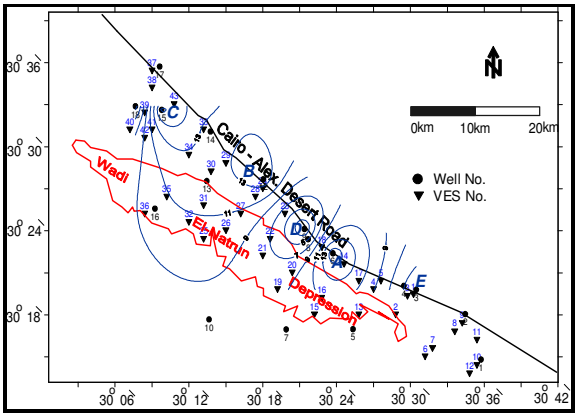

Figure (14) Effective thickness map of the second geoelectric layer from the well logging analysis.

b) Net and effective thicknesses maps of the third geoelectric layer

These maps (Figs. 15 & 16) are prepared to reflect the thinning and thickening of the effective zones through the third geoelectric layer. By this way, the thick and thin parts of this layer are mostly look like those of the mentioned one. Accordingly, the thick parts (A, B, C and D) and thin parts (E and F) occupy nearly similar locations to those of the second layer. The only exception is in the southeastward spreading of the thick part A, in a way vanishes the far southeastern thin part (E) of the second layer. Also, the thin part (F) is accentuated with respect to the two surrounding thick parts (B and D), in a way configuration the thick wide part (C) of the third layer as compared to the second one.

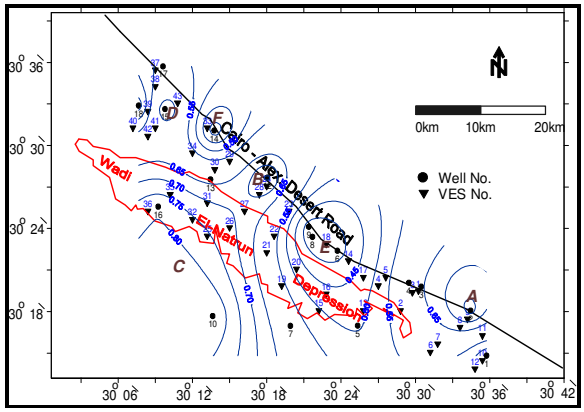

Figure (15) Net thickness map of the third geoelectric layer from the well logging analysis (after Ammar, 2002).

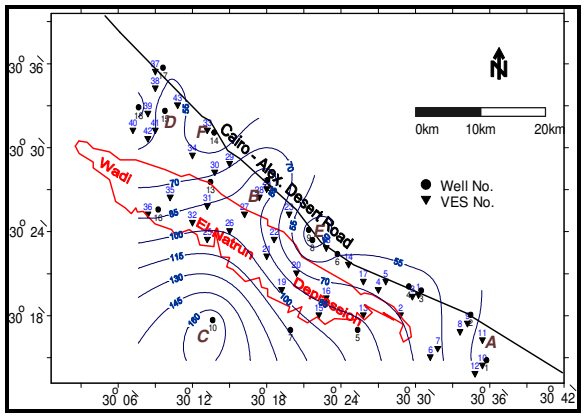

Figure (16) Effective thickness map of the third geoelectric layer from the well logging analysis.

c) Net and effective thicknesses maps of the fourth geoelectric layer

The net and effective thicknesses maps of this layer (Figs. 17 & 18), show two thin parts (B and C) subtending between them a thick one (A). The thin features occupy the southeastern and northwestern parts, while the thick one locates the central eastern part. By this way, the entire central part of the considered area is characterized by an intermediate gradient of dashed contours. This may be due the limitation of the penetrated electric current to the whole depth range of the fourth layer, in a way skips the details of the in-between net thickness features of positive and negative polarities.

Also, there is a general southeastward increase of the net thickness of this layer in a reversed direction to what happens for the second layer. However, the varied net thickness features distribution, beside the general net thickness reversal of the fourth layer, as compared to the second layer added a further evidence of check to the separation between the third and fourth geoelectric layers.

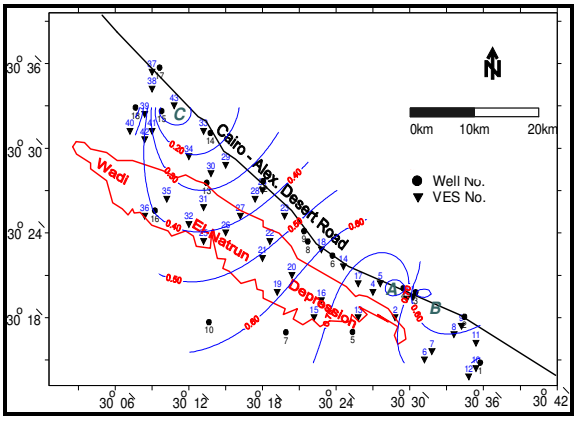

Figure (17) Net thickness map of the fourth geoelectric layer from the well logging analysis (after Ammar, 2002).

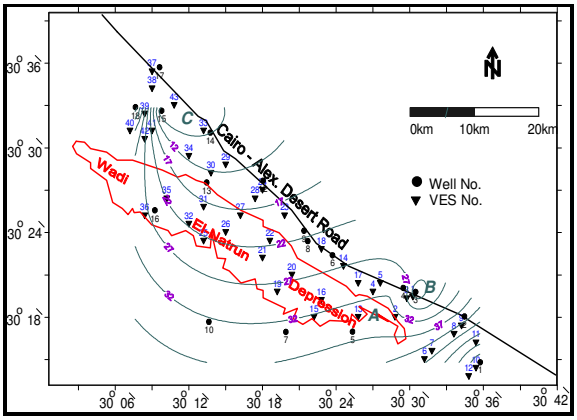

Figure (18) Effective thickness map of the fourth geoelectric layer from the well logging analysis.

4. The Relationship between True Resistivity (P_t Ω.M) and Water Saturation Percentage (S_w%)

The deduction of a relationship between the true resistivity and water saturation percentage was carried out by MINITAB statistical software package. This package was used for fitting the data to obtain an optimal estimation of the model's parameters. The outputs of this program were included the descriptive statistics, parameter estimation, statistical hypothesis testing and the basic linear regression, which consists of linear regression, analysis of variance (ANOVA) table and model fit validation. Then, by applying the previous statistical concepts, the relationship between the true resistivity and water saturation will be deduced, especially for the third geoelectric layer. Because the base of this layer was reached by the drilling wells and electric current, and also referred to the same constituents of Wadi El-Natrun aquifer, that includes the third and fourth geoelectric layers.

Generally, decreasing the resistivity of rocks gives an indication about the increase of water saturation into the pores of these rocks ($S_w \propto 1/\rho_t$). By judging the previous relationship, the distribution is normal and identical, the general trend of the data is linear and the model fit is valid. But, because the T and F values are high, the P-value is decreased to zero. This reflects that, the evidence between the two variables is strong and this relationship is different. The correlation between these variables is high (-0.884; P-value = 0.0), see Figure (19). There is a strong evidence of a relationship between both and this relationship is linear and it means that, S_w% differ significantly for different ρ_t (Ω.m). The R^2 of the two variables is around 78.1%, that refers to ρ_t (Ω.m) of Wadi El-Natrun aquifer/Pliocene fluvio-marine aquifer system in Wadi El-Natrun area can not be interpreted more than 78.1% of S_w% or around 21.9 of S_w% can not be interpreted by ρ_t (Ω.m). This resulted from the effect of shale distribution, connection and saturation of the pores of the aquifer, besides the effect of salinity on the conductivity of water in the pores. Hence, it can use the following linear regression for estimating S_w% from ρ_t (Ω.m):

$$S_w\% = 0.416652 \_ 0.00434\ \rho_t \quad \text{..... (5)}$$

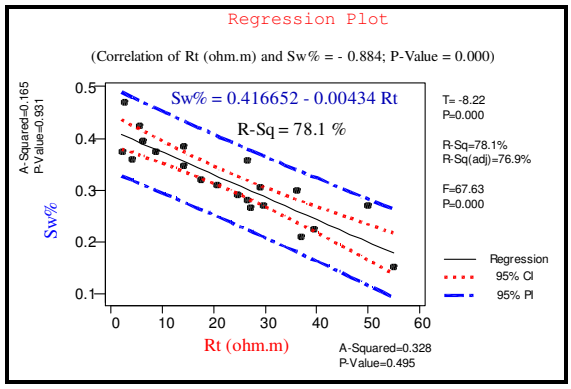

Figure (19) the relation between true resistivity and water saturation percentages of the third layer (Wadi El-Natrun aquifer).

5. Groundwater Potential

The amounts of groundwater for the evaluated geoelectric layers in the studied sections, generally, depend upon the thicknesses of the water-bearing layers, the thicknesses of the effective zones of the layers, the porosity which depends upon the lithology of the layers, and the water saturation percentages of the layers across the area of study.

Generally, the potentialities of groundwater for any layer give indication about the ability of any layer to produce specific amounts of groundwater, that depend on the fulfilling of the formerly established parameters. So, the assessment of the groundwater potentialities requires the construction of the water

saturation map and the net thickness and effective thickness variation maps of each analyzed layer in the studied section. In this respect, the evaluation will be primary confined to the second, third and the fourth geoelectric layers, which are collectively considered the shallow two aquifers.

II) Estimating the groundwater potential from the well logging and geoelectric analysis

From the comparison between the calculated total effective (T_{AV}) and net (T_{NAV}) thickness values from the well logging and geoelectric analyses, the following results in table (1) will be used for estimating the groundwater potential.

Table (1) Comparison between the calculated total effective and net thickness values estimated from the well logging and geoelectric analyses.

Geoelectric Layers	T_{AV} (m) (from Well Logging Analysis)	T_{AV} (m) (from Geoelectric Analysis)	T_{NAV} % (from Well Logging Analysis)	T_{NAV} % (from Geoelectric Analysis)
Second Layer	**18.56**	**19.12**	**0.416**	**0.488**
Third Layer	**110.3**	**107.23**	**0.581**	**0.662**
Fourth Layer	**71.7**	**87**	**0.52**	**0.63**

As shown earlier, estimating the groundwater potential of the evaluated layers requires the construction of the water saturation map to calculate the water percentages, the net thickness map to determine the thickness variations and the effective thickness map to determine the effective thickness variations of the clastic zones, that are saturated with water. These will be achieved for the second, third and fourth geoelectric layers at the study area.

To estimate the groundwater volume (V_w), the following equations will be used for calculating the groundwater amounts as follow:

when $S_w = \frac{V_w}{V_p}$ ……..…..… (6)

and $\phi_T = \frac{V_P}{V_T}$ ……..…..…… (7)

(Serra, 1984)

where: V_w is the volume (amount) of water.

V_P is the volume of all the empty spaces (occupied by water).

V_T is the total volume of the rock.

ϕ_T is the total porosity; consists of all the void spaces (pores, channels, fissures and vugs) between the solid components.

Then, from equations 6 & 7:

$V_p = \frac{V_w}{S_w}$ ……..... (8)

and $V_p = \phi_T * V_T$ ……..…..…… (9)

Also, from equations 8 & 9:

When $V_p = V_p$

$\frac{V_w}{S_w} = \phi_T * V_T$ ……..…..... (10)

Then $V_w = \phi_T\% * V_T * S_w\%$ ……..…..… (11)

When $V_T = L * W * T_{av}$ ……..…..… (12)

And $V_E = V_T * T_{Nav}\%$……..…..…… (13)

Hence, based on the above mentioned equations, the present author modified and illustrated how to derive an equation relating $\phi_T\%$, (V_T, $T_{Nav}\%$) or V_E, $S_w\%$, can be used regionally to estimate the volume (amount) of water (V_w) in site as shown as follow:

$V_w = \phi_T\% * V_T * T_{Nav}\% * S_w\%$..……..…….... (14)

Or $V_w = \phi_T\% * V_E * S_w\%$ ……..…..…..(15)

where: V_T is the total volume of the average thickness of the evaluated layer.

L is the length of the evaluated layer along the area of study.

W is the width of the evaluated layer across the area of study.

T_{av} is the average thickness of the effective zones of the evaluated layer.

V_E is the effective thickness volume of the evaluated layer.

$T_{Nav}\%$ is the net thickness average of the effective zones of the evaluated layer.

$\phi_T\%$ is the porosity of lithology of the evaluated layer.

$S_w\%$ is the water saturation percentage of the evaluated layer.

i- Estimating the groundwater volume of the second geoelectric layer

By applying the last equations (12 - 15) and substituting the input values of this layer (Table 2), where: L =9cm, W =2cm, S_{wav}=0.373%, Scale factor= $\left(\frac{1000}{1.45}\right)^2$ = 47562426 m^2

Table (2) Comparison between the estimated groundwater volume of the second layer from the well logging and geoelectric analyses.

Input and output parameters	T_{av} (m)	T_{Nav} %	V_T (m^3)	V_E (m^3)	V_w (m^3) When ϕ=10%	V_w (m^3) When ϕ=20%
From well logging analysis	**18.56**	**0.416**	**1.5889655^{10}**	**6.6100966^{09}**	**2.465566^{08}**	**4.931132^{08}**
From geoelectric analysis	**19.12**	**0.488**	**1.6369084^{10}**	**7.9881132^{09}**	**2.9795662^{08}**	**5.9591324^{08}**

ii- Estimating the groundwater volume of the third geoelectric layer

From the application of the last equations (12 - 15) and substituting the input values of this layer (Table 3), where: L =9.5cm, W =2.7cm, S_{wav}=0.393%, Scale fact.= 47562426 m^2

Table (3) Comparison between the estimated groundwater volume of the third layer from the well logging and geoelectric analyses.

Input and output parameters	T_{av} (m)	T_{Nav} %	V_T (m^3)	V_E (m^3)	V_w (m^3) When ϕ=10%	V_w (m^3) When ϕ=20%
From well logging analysis	110.3	0.581	1.3456338^{11}	7.8181322^{10}	3.072526^{09}	6.1450519^{09}
From geoelectric analysis	107. 3	0.662	1.3081805^{11}	8.6601549^{10}	3.4034409^{09}	6.8068818^{09}

iii- Estimating the groundwater volume of the fourth geoelectric layer

Also, from the application of the last equations (12-15) and substituting the input values of this layer (Table 4), Where: L =9cm, W =2.3cm, S_{wav}=0.428%, Scale factor= 47562426 m^2

Table (4) Comparison between the estimated groundwater volume of the fourth layer from the well logging and geoelectric analyses.

Input and output parameters	T_{av} (m)	T_{Nav} %	V_T (m^3)	V_E (m^3)	V_w (m^3) When ϕ=10%	V_w (m^3) When ϕ=20%
From well logging analysis	71.1	0.52	7.0591677^{10}	3.6707672^{10}	1.5710884^{09}	3.1421767^{09}
From geoelectric analysis	87	0.63	8.5655173^{10}	5.3962759^{10}	2.3096061^{09}	4.6192121^{09}

Finally; from the above mentioned results, that depend essentially on the effective thickness and net thickness variations of the three water-bearing layers (second, third and fourth geoelectric layers) and when the porosity (ϕ) is assumed to be 10% and 20%, it can be concluded that, the groundwater potential of the third layer is better than that of the fourth layer, and these in-turn are far better than that of the second layer for the shallow aquifer of the studied area. So, water productivity is ranked by the same way when the water wells are drilled in this area.

Unfortunately, the lack of porosity tools (density, sonic and neutron logs) from the well logging data of this area makes it difficult to determine accurately the rock porosities of the assessed layers, consequently defining more realistic figures about the amounts, potential and productivity of the groundwater for this shallow aquifer of Wadi El-Natrun area of the northeastern part of the Western Desert of Egypt.

6. Summary and Conclusions:

The interpretation of forty-three geoelectric stations added to the analysis of resistivity, SP and gamma-ray logs of fifteen water wells were used for determining the expected subsurface geologic and hydrogeologic features of the water-bearing deposits and to estimate the groundwater potential of Wadi El-Natrun area.

The geoelectric interpretation, carried out through ZOHDY'S method and RINVERT'S method, referred to the number of detected layers is varied from three to fives, and their resistivities are ranged between very low (2Ω.m) and high values (982.5Ω.m), and the thicknesses are varied from (0.9m) to (197.3m). The lithology of *the first layer* consists of sand, gravel and rock fragments; *the second layer* is formed from marly and shaly sand, and include lenses of shale; *the third layer* is made up of clayey and sandy gravel and changed to clay; *the fourth layer* is composed of clayey sand and gravel, and the fifth layer is constituted from sandstone. The layers from the second to the fifth have varying amounts of groundwater, where the second layer is dated to Quaternary period and the third to the fifth layers are belonged to the Tertiary period. These layers revealed the presence of unconfined Nile Delta aquifer of the second layer; confined and unconfined Wadi El-Natrun aquifer (Pliocene aquifer) of the third and fourth layers, and the Moghra aquifer (Lower Miocene aquifer) of the fifth layer. The second to the fourth layers were under consideration in estimating the groundwater potential of the area.

Estimating the groundwater volume of these layers was required through the construction of water saturation, net thickness and effective thickness of the clastic zones, that hold free water. From the geoelectric analysis, the net and effective thickness maps of the second to the fourth layers were constructed by using the true resistivity values in separating and excluding the thicknesses of low water content and high volumes of shale. These maps reflected the increase of the effective zones in the sites B and E of the second layer, the site E of the third layer and the site B of the fourth layer.

From the interpretation of the well log data of fifteen water wells, the shale content, matrix content, water saturation, net thickness of the water-bearing layers of the second, third and fourth layers were evaluated petrophysically. The water saturation maps are referred to the site B at the second layer, site C at the third layer and site A at the fourth layer reflect high water saturation percentages. Also, the net and effective thickness maps of the fore-mentioned layers reveal three thickening sites A, B and C at the southeastern and northwestern parts of the second layer, four thickening sites A, B, C and D at the third layer, while there is only one thick site A locates the central eastern part of the fourth layer.

The construction of the relationship between the true resistivity (ρ_t Ω.m), derived from the

geoelectric analysis, and water saturation (S_w%), extracted from the well logging analysis, was restricted only to the third layer by using MINITAB statistical program. From the statistical analysis of the previous parameters, the water saturation percentage can be calculated from the true resistivity, when the well logging data are missed.

From the comparison between the calculated net and effective thickness values derived from the geoelectric interpretation and well logging analysis, it is appeared that, there is a small discrepancy between the estimated values. Then, from the application of the resulted mathematical equations for calculating the groundwater potential, the maximum volume of groundwater was contained at the third layer, then followed by the fourth layer and then came the second layer. This reveals that, the best layer which has high groundwater potentialities is the third layer, followed by those of the fourth layer, while the potentialities of the groundwater of the second layer are low. The estimated water quantities for these layers, assuming porosity of 10% were 3.4034409^{09} m^3, 2.3096061^{09} m^3 and 2.9795662^{08} m^3 from the geoelectric interpretation, and were 3.072526^{09} m^3, 1.5710884^{09} m^3 and 2.465566^{08} m^3 from the well logging analysis.

At the end, from the previous outputs, the geoelectric data can be used for estimating the groundwater potential in case of having the same geological features and when the well log data are not available.

Corresponding author
Dr. Abdallah Ibrahim Ammar
Research Institute for Groundwater National Water Research Center El-Kanater El-Khairiya, Cairo, Egypt

7. References:

1. Ammar, A.I., 2002: Geophysical studies on groundwater reservoir in Wadi El-Natrun area, western desert, Egypt. M.Sc., Thesis, Fac., Sci., Ain Shams University, Egypt, 129p.
2. Cairo University/GARPAD, 1985: Groundwater resources evaluation of West Delta aquifer systems. Final report, Cairo, Egypt.
3. Dobrin, M.B., 1980: Introduction to geophysical prospecting. New York, MC. Graw-Hill. CO., 620p.
4. El-Fayoumy, I.F., 1964: Geology of groundwater supplies in Wadi El-Natrun area. M.Sc., Thesis, Fac., Sci., Cairo University, Egypt, 200p.
5. Keys, W.S., 1990: Borehole geophysics applied to groundwater investigations: Techniques of water-resources investigations of the United States Geological Survey. BK.2, Ch. E2, 1-9.
6. MINITAB, 1998: Statistical software package. Licensed to analysis of the statistical environmental data.
7. RIGW, 1990: Hydrogeological map of Egypt report, Scale 1: 100,000. First edition.
8. RIGW/IWACO, 1990b: Hydrogeological inventory and groundwater development plan Western Nile Delta region. TN 77.01300-90-02.
9. Rinvert, 1999: Geophysical software package: Licensed to hydrogeology and engineering geology. Hochi Minh City-Vietnam., Reg., Number, RW 140032, February 03, 1999.
10. Said, R., 1981(a): The geology of Egypt. Balkema, Rotterdam, 289p.
11. Said, R. (ed), 1990: The geology of Egypt. Balkema, Rotterdam, 733p.
12. Serra, O., 1984: Fundamental of well-log interpretation: The acquisition of logging data, developments in petroleum science. 15A-trans., El Sevier Science Publishers B.V., Amsterdam, the Netherlands, Vol.1, 413p.
13. Schlumberger, 1972: Log interpretation. Vol.1, principles.
14. Sharma, P.V., 1997: Environmental and engineering geophysics. Cambridge Univ. press, United Kingdom, ISBN 0-521-57240-1, 207-261pp.
15. Shata, A.A., and El-Fayoumy, I.F., 1968: Geomorphological and morphopedological aspects of the region west of the Nile Delta with reference to Wadi El-Natrun. Desert Inst., Bull., 17 NO1.
16. Stanislav, M., et al., 1984: Introduction to applied geophysics Faculty of Science, charales University, Prague, 547p.
17. Telford, W.M., Geldart, L.P., Sheriff, R.E., and Key, I.P., 1990: Applied geophysics. Cambridge University press, New York. 632-701pp.
18. Zohdy, A.A.R., and Bisdorf, R.J., 1989: Schlumberger sounding data processing and interpretation program. U.S., Geological Survey, Denver, Co.